

Grating-like Terahertz Metasurface for Large-Deflection-Angle Beam Manipulations

Yuan Fu ^{1,†}, Xiaojian Fu ^{1,2,*,†}, Lei Shi ¹ and Tie Jun Cui ^{1,2,*}¹ State Key Laboratory of Millimeter Waves, Southeast University, Nanjing 210096, China² Institute of Electromagnetic Space, Southeast University, Nanjing 210096, China

* Correspondence: fuxj@seu.edu.cn (X.F.); tjcui@seu.edu.cn (T.J.C.)

† These authors contributed equally to this work.

Abstract: Multifunctional terahertz beam manipulations have attracted much attention because of the potential for wide-scale applications in terahertz imaging, communications, etc. In this work, a grating-like terahertz reflective-type metasurface is designed for terahertz beam manipulations on the basis of a frequency-scanning mechanism. The theoretical calculation based on the grating principle has predicted that the metasurface grating can steer the deflected beam from 59.5° to 47.3° as the frequency of the perpendicularly incident terahertz wave changes between 0.87 and 1.02 THz. The large-deflection-angle frequency-scanning performance is validated by both numerical simulations and experimental tests. The metasurface grating developed in this work possesses the potential for applications in terahertz beam steering and beam-splitting devices.

Keywords: metasurface; terahertz; grating; frequency-scanning



Citation: Fu, Y.; Fu, X.; Shi, L.; Cui, T.J. Grating-like Terahertz Metasurface for Large-Deflection-Angle Beam Manipulations. *Appl. Sci.* **2022**, *12*, 12322. <https://doi.org/10.3390/app122312322>

Academic Editor: Adel Razek

Received: 31 October 2022

Accepted: 29 November 2022

Published: 2 December 2022

Publisher's Note: MDPI stays neutral with regard to jurisdictional claims in published maps and institutional affiliations.



Copyright: © 2022 by the authors. Licensee MDPI, Basel, Switzerland. This article is an open access article distributed under the terms and conditions of the Creative Commons Attribution (CC BY) license (<https://creativecommons.org/licenses/by/4.0/>).

1. Introduction

The terahertz band refers to the electromagnetic wave between microwave and far-infrared waves, which is commonly defined from 0.1 to 10 THz [1]. Over the past few decades, the promising application prospects of terahertz technology in wireless communication [2], remote sensing [3], imaging [4,5], biomedicine [6], and moving-target detection [7] have drawn increased research interest. As the essential components, terahertz electromagnetic devices such as beam-steering antennas [8], polarization converters [9], and high-Q resonators [10] have been widely reported. Among these, multifunctional beam manipulations, especially beam steering, have received much interest [11,12]. Beam-steering technologies usually include mechanical scanning, phased array, frequency scanning, and multi-feed technologies [11]. In the terahertz band, frequency-scanning technology may have the advantages of high response speed, low power consumption, and a simple system compared with the other three mechanisms.

Recently, a frequency-scanning antenna was designed for the W band for real-time imaging. The imaging system operating at 79 GHz was composed of a frequency-scanning array, a parabolic reflector, and a post-processing module, which proved its feasibility for low-cost imaging applications [13]. A frequency-sweep reflector antenna working at 235–330 GHz was proposed based on the direction-of-arrival estimation mechanism [14]. The diffraction enhancement method is applied to design the antenna structure to attain high gain and directivity, and the measured results show that the diffraction beam steers from -36.6° to -11.03° during the designed operating frequency. A two-dimensional frequency-scanning planar-integrated array based on the leaky wave principle and true-time-delay phase-shifting feeding network was designed and manufactured, and consequently, a scanning range of $22.7^\circ \times 60^\circ$ is achieved by sweeping the frequency between 325 and 400 GHz [15].

Moreover, metasurfaces, especially reconfigurable and programmable metasurfaces, have provided considerable freedom for manipulating terahertz beams [16–21]. Phase-change materials and electrically tunable materials were extensively exploited for developing dynamically controlled metasurface elements. For instance, by varying the temperature, a frequency-tunable metasurface filter and ultra-wideband absorber based on the phase-change material vanadium dioxide were designed, respectively [22,23]. A dual-band terahertz absorber has been designed using a graphene-based metamaterial resonator, and tunable absorption performances can be attained by changing the chemical potential of graphene [24]. Nematic liquid crystal (LC) with a birefringence effect has also drawn a lot of attention. The LC-based metal–dielectric–metal structure has been designed and fabricated to modulate the reflection phase of electromagnetic waves fully electronically in millimeter frequencies [25]. A transmissive terahertz amplitude modulator working at 421.2 GHz was implemented based on an LC-loaded plasmonic metamaterial, and a large modulation depth of up to 96% can be obtained by applying different bias voltages to the LC layer [26]. Tunable terahertz beam-steering was realized by using LC-coupled reconfigurable metasurfaces [27]. In terms of programmable metasurfaces, LC-based dynamically programmable reflective and transmissive metasurfaces were achieved at 672 GHz and 408 GHz, respectively [28,29], and the programmable modulation of terahertz beams can be performed. Furthermore, a wide-angle beam scanning device using a 1-bit field programmable terahertz metasurface was developed with a working frequency covering 630–650 GHz and a scanning beam ranging from 20° to 60° [30]. However, terahertz frequency-scanning metasurfaces have not been widely investigated, especially for large-deflection-angle beam control.

In this paper, a reflective grating-like metasurface is developed to realize frequency-controlled beam-steering. By designing the metasurface elements, we obtain a reflective frequency-scanning metasurface operating in the optimized frequency range of 0.87–1.02 THz. The measured diffraction angles are in good agreement with the theoretical calculations and simulations.

2. Principle and Design

The working principle of the grating-like beam-sweeping metasurface will be discussed in detail. As shown in Figure 1, the metasurface grating is a kind of multilayer structure, among which the key functional layers are the metallic structural layer, which is composed of periodic metasurface elements and slits, the LC layer, and the ground layer. It is noted that the metasurface element is designed with a typical subwavelength structure of a complementary split-ring resonator (CSRR). There is a slit between every two elements whose width is much smaller than the length of the metasurface element, and hence the metasurface exhibits the grating effect. In the geometry of Figure 1, the plane parallel to the metasurface is set as the XOY plane. The period of metasurface grating was described by the grating constant D_x . As the plane electromagnetic wave with an x polarization is incident onto the metasurface grating, the diffraction waves of different orders will be generated, which can be described by the following diffraction equation:

$$\sin \theta \pm \sin \theta_0 = m \frac{\lambda}{D_x} \quad (m = 0, \pm 1, \pm 2, \pm 3 \dots) \quad (1)$$

where θ_0 and θ represent the orientation angles of the incident wave and the diffraction wave, respectively, λ is the free-space wavelength, D_x represents the grating constant, and m denotes the diffraction order, which is an integer. Since the incident wave is perpendicular to the metasurface grating in this scheme, θ_0 is equal to zero, then Equation (1) can be rewritten as [31]

$$\theta = \sin^{-1} \left(\frac{m\lambda}{D_x} \right) \quad (m = 0, \pm 1, \pm 2, \pm 3 \dots) \quad (2)$$

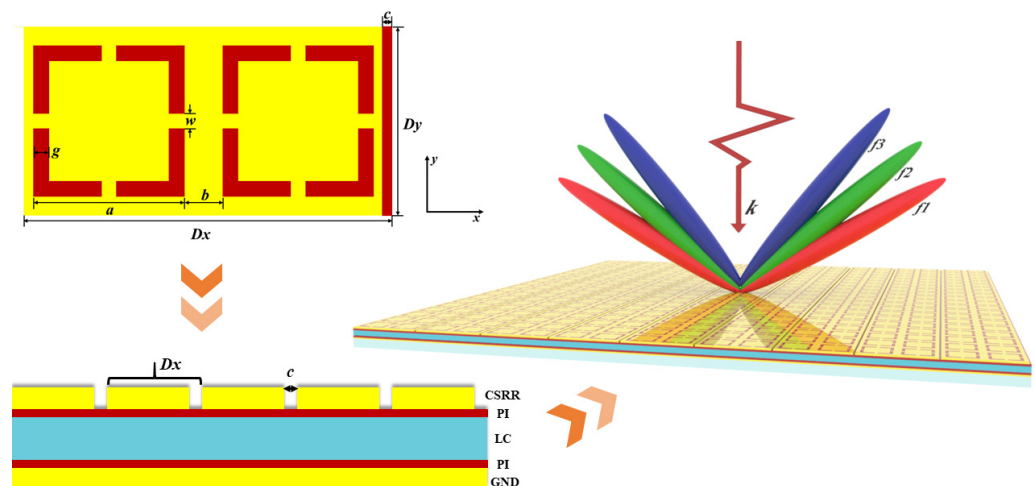


Figure 1. Schematic configuration of the metasurface grating. The geometric parameters of the unit cell are as follows: $a = 160 \mu\text{m}$, $b = 40 \mu\text{m}$, $c = 6 \mu\text{m}$, $g = 16 \mu\text{m}$, $w = 16 \mu\text{m}$, $D_x = 400 \mu\text{m}$, and $D_y = 200 \mu\text{m}$. The metasurface consists of seven layers, which from top to bottom, are quartz, complementary split-ring resonator (CSRR), Polyimide (PI), liquid crystal (LC), PI, metal ground, and silicon substrate. The thickness of the metal layer (gold), PI, and LC are 300 nm , 90 nm , and $45 \mu\text{m}$, respectively. Silicon substrate and ultrathin quartz (which are not shown in the schematic) are used to support the metal ground and metallic CSRR, respectively, and PI layers engineered with parallel grooves are contributed to the pre-orientation of liquid crystal molecules.

Equation (2) is the simplified expression of Equation (1) under the case of normal incidence. As the diffraction order m is equal to zero, we can obtain the 0th diffraction beam at $\theta = 0^\circ$. For $m = \pm 1$, the ± 1 st diffraction beams can be obtained, and the diffraction angle is frequency (or wavelength) dependent, which reflects the dispersion characteristic of the grating. Moreover, for a fixed working frequency, the diffraction beams of different orders (0th, ± 1 st, ± 2 nd, etc.) can also be determined by Equation (2). Additionally, hence, Equation (2) describes the diffraction behavior of a one-dimensional grating under normal incidence. As observed in Figure 1, a series of diffraction waves will be generated at the XOZ plane by the metasurface grating, and the diffraction angle is frequency-dependent.

It is interesting to note that the metasurface designed in this work is a multifunctional beam-manipulating device. In our previous work [30], terahertz beam scanning was achieved based on the electrically controlled programmable metasurface. Specifically, the digital coding states of the LC-loaded metasurface elements can be rapidly switched by tuning the bias voltage applied to the LC molecules, and then the coding pattern can be modulated in real-time, which leads to programmable beam manipulation. Nevertheless, herein, it functions as a frequency-scanning device, and no bias voltage is required.

According to Equation (2), the diffraction angles for terahertz waves of different frequencies and orders can be calculated. The grating constant is $400 \mu\text{m}$. Due to the weak intensity of high-order diffraction waves, we only consider the first-order diffraction case. Moreover, the optimized working frequency range was determined to be $0.87\text{--}1.02 \text{ THz}$ according to the subsequent numerical simulation and experimental results. Table 1 presents the incident frequencies and the corresponding diffraction angles calculated based on Equation (2). It can be observed that the diffraction angle can reach up to 59.5° as the incident frequency is equal to 0.87 THz , and it ranges from 59.5° to 47.3° as the frequency increases. The large beam-deflection angle is mainly owing to the subwavelength metasurface element and the resultant large values of the ratio of working wavelength to the grating constant.

Table 1. Diffraction angles calculated at different incident wave frequencies.

Incident Frequency/THz	Diffraction Angle/Degree	Incident Frequency/THz	Diffraction Angle/Degree
0.87	± 59.5	0.95	± 52.1
0.88	± 58.5	0.96	± 51.4
0.89	± 57.4	0.97	± 50.6
0.90	± 56.4	0.98	± 49.9
0.91	± 55.5	0.99	± 49.3
0.92	± 54.6	1.00	± 48.6
0.93	± 53.8	1.01	± 48.0
0.94	± 52.9	1.02	± 47.3

3. Results and Discussion

Full-wave simulation of the metasurface grating is performed in the commercial software, CST Microwave Studio, to verify our theoretical calculations. As an example, we present the three-dimensional (3D) and one-dimensional (1D) far-field radiation patterns at 0.87 THz. As can be seen in Figure 2a,b, in addition to the zero-order diffraction beam, two first-order diffraction beams are generated at $\pm 59.2^\circ$ for the perpendicularly incident terahertz plane wave. The normalized amplitude of the first-order diffraction waves to that of the zero-order diffraction beam is -9.49 dB. As for comparison, the far-field radiation patterns of the grating constructed by metallic strips with the same grating constant and slit width were also shown (see Figure 2c,d). Obviously, the CSRR-based grating has a higher intensity for the first-order diffraction beams, and hence CSRR structure is employed to construct the metasurface grating to obtain a high diffraction efficiency. The data for the diffraction angles at various operating frequencies can be extracted from the simulated far-field scattering patterns of the grating.

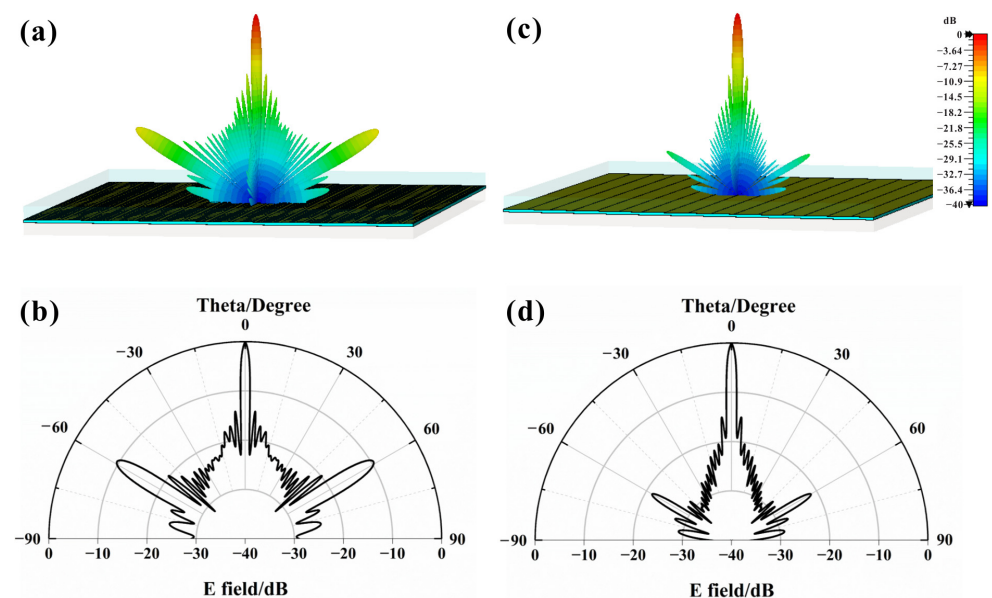


Figure 2. The far-field radiation patterns for (a,b) CSRR-based metasurface grating and (c,d) metallic strip-based grating at 0.87 THz. (a,c) 3D far-field patterns; (b,d) 1D far-field patterns. In simulation, both the two 1D gratings have 16 lines.

The metasurface grating sample is fabricated using lithography technology, and the size of the grating is $12.8 \text{ mm} \times 12.8 \text{ mm}$ (32 lines). Figure 3a presents the optical micrograph of the fabricated metasurface grating. It can be found that the measured grating constant is around $404.2 \mu\text{m}$, close to the design value. The far-field radiation patterns of the reflective metasurface grating are measured on a terahertz time-domain spectroscopy mea-

surement system. More details of the fabrication and experiments can be found in Ref. [30]. Figure 3b,c show the relationship between the reflection angle and terahertz amplitude under different frequencies (B-spline curves for the measured points). It can be obviously observed that the diffraction angle varies with the working frequency. Specifically, when the scanning frequency ranges from 0.87 to 1.02 THz, the corresponding scanning angle will be steered from 58.7° to 48.0° for the +1st order diffraction wave and from -56.7° to -46.2° for the -1st order diffraction wave, respectively. The two diffraction beams at the same frequencies are not strictly symmetric, which can probably be ascribed to the error of orientation angle between the incident terahertz beam and the metasurface sample, as well as the measurement error of the diffraction angle induced by beam broadening.

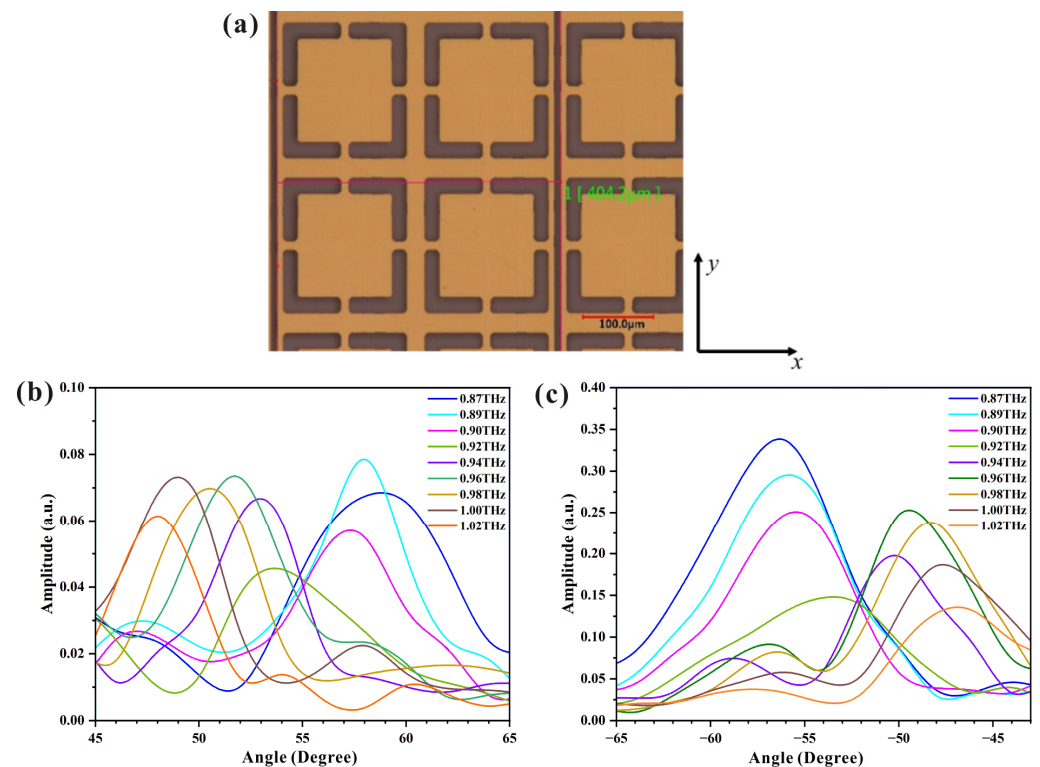


Figure 3. (a) The optical micrograph of the fabricated metasurface grating; the measured results of the diffraction wave. (b) +1st order mode; (c) -1st order mode.

Figure 4 shows the comparison among the theoretical, simulated, and measured scanning angles of the +1st order diffraction wave covering the frequency range of 0.87–1.02 THz. It can be found that the simulation angles of the diffraction waves are consistent with the theoretical angles in the designed frequency band. The measured diffraction angles also agree well with the theoretical results except for the frequency point at 0.92 THz, where a slight deviation of around 1.2° can be observed. Possible reasons for the deviations between the experimental and theoretical data are as follows: on the one hand, dimensional deviations of metasurface structure induced by the fabrication error will lead to the deviation of diffraction angle; on the other hand, the beam reflected by the sample will be broadened as a result of fabrication error and non-uniform thickness of quartz substrate, which will also contribute to the deviation in the angle measurement. The measured beam scanning range is around 10.7° for the +1st order diffraction mode in the 0.87–1.02 THz band, which is slightly smaller than the theoretical value of 12.2° .

We remark that a liquid-crystal (LC) layer was embedded into the metasurface element as a dielectric spacer. The LC layer contributes to the performance of the large deflection angle of the metasurface grating to some extent, as the loading of LC induces the redshift of the effective working frequency band of the metasurface grating (compared to the air

with the same thickness) [32,33], which will lead to the increased deflection angle according to Equation (2). In addition, LC possesses the electrically tunable dielectric constant, and hence the switchable grating effect can be expected in this LC metasurface grating. More importantly, we wish to develop a kind of bifunctional metasurface device, that is, the metasurface behaves as an electrically controlled programmable metasurface in the low-frequency portion of the y -polarized incident wave and functions as a frequency-scanning grating in the high-frequency band for the x -polarized incident wave. Thus, we also utilize the LC-integrated metasurface structure in this work.

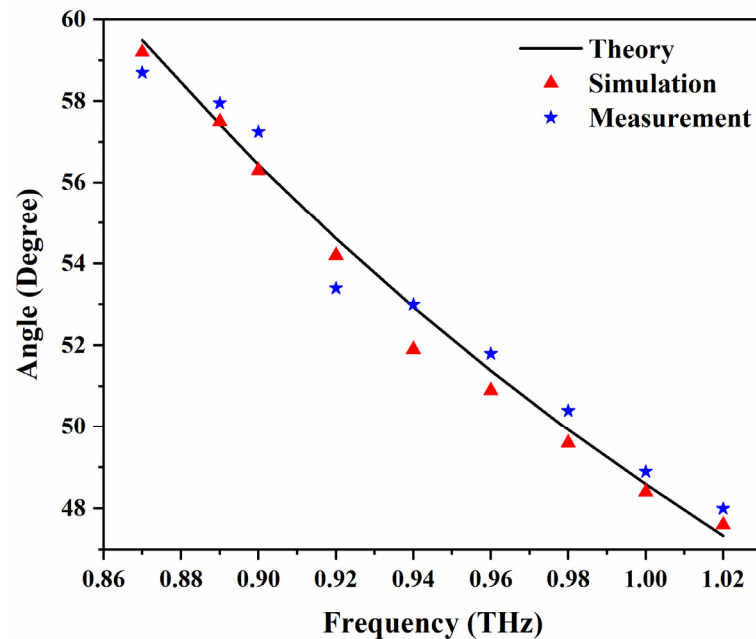


Figure 4. The measured results of the diffraction wave (+1st order mode) compared with the theoretical and simulated results.

According to the aforementioned analyses, the grating-like metasurface can steer the terahertz beams in a large deflection-angle region, which indicates the potential applications in terahertz frequency-scanning antennas. Compared with phased-array antennas, frequency-scanning antennas commonly possess higher response speeds and lower energy consumption. Additionally, the metasurface can also be applied to beam splitting. At optical frequencies, beam-splitting prisms and gratings are usually utilized to design beam splitters based on the dispersion effect, which is widely used in spectrometers. Nevertheless, in the terahertz regime, beam-splitting components are not widely reported. Thus, the grating-like metasurface can be extended to terahertz spectral separation. It is worth noting that the working bandwidth can be further broadened by designing multilayer devices or constructing composite metasurfaces consisting of sub-lattices with different operating frequency bands. Additionally, hence, broadband terahertz spectral separation can probably be achieved based on metasurface grating.

4. Conclusions

A frequency-scanning metasurface grating operating in the terahertz band has been designed and manufactured. The metasurface grating shows a large diffraction angle of up to 59.5° and an angle range of $\pm(59.5\text{--}47.3^\circ)$ as the working frequency varies in the range of 0.87–1.02 THz. It is also numerically demonstrated that the metasurface grating based on CSRR has higher first-order diffraction intensity compared with metallic strip grating with the same grating constant and slit width. The experimentally measured diffraction angles are in good agreement with the theoretical and simulated results. Moreover, the proposed reflective grating-like metasurface shows the functions of beam scanning and

beam splitting and has important applications in the fields of moving target detection, wireless communication, spectral separation, and other fields.

Author Contributions: Conceptualization and supervision, X.F. and T.J.C.; software, Y.F. and L.S.; validation, X.F., Y.F. and L.S.; writing—original draft preparation, Y.F.; writing—review and editing, X.F. and T.J.C. All authors have read and agreed to the published version of the manuscript.

Funding: This research was funded in part by the National Key Research and Development Program of China (Grant Nos. 2018YFB1801505, 2017YFA0700201, 2017YFA0700202, and 2017YFA0700203), in part by the National Natural Science Foundation of China (Grant Nos. 61871127, 61735010, 61731010, 61890544), and in part by the 111 Project (Grant No. 111-2-05).

Data Availability Statement: The data presented in this study are available upon request from the corresponding authors.

Conflicts of Interest: The authors declare no conflict of interest.

References

1. Ferguson, B.; Zhang, X.-C. Materials for terahertz science and technology. *Nat. Mater.* **2002**, *1*, 26–33. [[CrossRef](#)] [[PubMed](#)]
2. Moon, S.R.; Kim, E.S.; Sung, M.; Rha, H.Y.; Lee, E.S.; Lee, I.L.; Park, K.H.; Lee, J.K.; Cho, S.H. 6G Indoor Network Enabled by Photonics-and Electronics-Based sub-THz Technology. *J. Lightwave Technol.* **2022**, *40*, 499–510. [[CrossRef](#)]
3. Xin, F.F.; Su, H.Y.; Xiao, Y. Terahertz Imaging System for Remote Sensing and Security Applications. In Proceedings of the 3rd Asia-Pacific Conference on Antennas and Propagation (APCAP), Harbin, China, 26–29 July 2014; pp. 1335–1338.
4. Stantchev, R.I.; Yu, X.; Blu, T.; Pickwell-MacPherson, E. Real-time terahertz imaging with a single-pixel detector. *Nat. Commun.* **2020**, *11*, 2535. [[CrossRef](#)] [[PubMed](#)]
5. Fan, K.; Suen, J.Y.; Liu, X.; Padilla, W.J. All-dielectric metasurface absorbers for uncooled terahertz imaging. *Optica* **2017**, *4*, 601–604. [[CrossRef](#)]
6. Zaytsev, K.I.; Dolganova, I.N.; Chernomyrdin, N.V.; Katyba, G.M.; Gavdush, A.A.; Cherkasova, O.P.; Komandin, G.A.; Shchedrina, M.A.; Khodan, A.N.; Ponomarev, D.S.; et al. The progress and perspectives of terahertz technology for diagnosis of neoplasms: A review. *J. Opt.* **2020**, *22*, 013001. [[CrossRef](#)]
7. Li, H.; Li, C.; Wu, S.; Zheng, S.; Fang, G. Adaptive 3D Imaging for Moving Targets Based on a SIMO InSAR Imaging System in 0.2 THz Band. *Remote Sens.* **2021**, *13*, 782. [[CrossRef](#)]
8. Wu, B.; Hu, Y.; Zhao, Y.T.; Lu, W.B.; Zhang, W. Large angle beam steering THz antenna using active frequency selective surface based on hybrid graphene-gold structure. *Opt. Express* **2018**, *26*, 15353–15361. [[CrossRef](#)]
9. Yu, F.Y.; Zhu, J.B.; Shen, X.B. Tunable and reflective polarization converter based on single-layer vanadium dioxide-integrated metasurface in terahertz region. *Opt. Mater.* **2022**, *123*, 111745. [[CrossRef](#)]
10. Ding, C.F.; Jiang, L.K.; Wu, L.; Gao, R.M.; Xu, D.G.; Zhang, G.Z.; Yao, J.Q. Dual-band ultrasensitive THz sensing utilizing high quality Fano and quadrupole resonances in metamaterials. *Opt. Commun.* **2015**, *350*, 103–107. [[CrossRef](#)]
11. Fu, X.J.; Yang, F.; Liu, C.X.; Wu, X.J.; Cui, T.J. Terahertz Beam Steering Technologies: From Phased Arrays to Field-Programmable Metasurfaces. *Adv. Opt. Mater.* **2020**, *8*, 1900628. [[CrossRef](#)]
12. Qi, Y.; Zhang, B.; Ding, J.; Zhang, T.; Wang, X.; Yi, Z. Efficient Manipulation of Terahertz waves by multi-bit Coding Metasurfaces and its further application. *Chin. Phys. B* **2020**, *30*, 024211. [[CrossRef](#)]
13. Larumbe, B.; Laviada, J.; Ibáñez-Loinaz, A.; Teniente, J. Real-Time Imaging with Frequency Scanning Array Antenna for Industrial Inspection Applications at W band. *J. Infrared Millim. Terahertz Waves* **2017**, *39*, 45–63. [[CrossRef](#)]
14. Li, S.; Hou, P.; Zhang, P.; Hao, C.; Qu, J.; Jia, Q.; Li, G.; Li, C. Design of terahertz frequency scanning reflector antenna and its application in direction-of-arrival estimation. *J. Eng.* **2019**, *2019*, 7223–7227. [[CrossRef](#)]
15. Yao, S.S.; Cheng, Y.J.; Wu, Y.F.; Yang, H.N. THz 2-D Frequency Scanning Planar Integrated Array Antenna With Improved Efficiency. *IEEE Antennas Wirel. Propag. Lett.* **2021**, *20*, 983–987. [[CrossRef](#)]
16. Ding, L.; Luo, X.S.; Cheng, L.; Thway, M.; Song, J.F.; Chua, S.J.; Chia, E.E.M.; Teng, J.H. Electrically and Thermally Tunable Smooth Silicon Metasurfaces for Broadband Terahertz Antireflection. *Adv. Opt. Mater.* **2018**, *6*, 1800928. [[CrossRef](#)]
17. Fan, K.B.; Zhang, J.D.; Liu, X.Y.; Zhang, G.F.; Averitt, R.D.; Padilla, W.J. Phototunable Dielectric Huygens' Metasurfaces. *Adv. Mater.* **2018**, *30*, 1800278. [[CrossRef](#)] [[PubMed](#)]
18. Gorecki, J.; Piper, L.; Noual, A.; Mailis, S.; Papasimakis, N.; Apostolopoulos, V. Optically Reconfigurable Graphene/Metal Metasurface on Fe:LiNbO3 for Adaptive THz Optics. *ACS Appl. Nano Mater.* **2020**, *3*, 9494–9501. [[CrossRef](#)]
19. Ren, B.; Feng, Y.X.; Tang, S.; Wang, L.; Jiang, H.; Jiang, Y.Y. Dynamic control of THz polarization modulation and multi-channel beam generation using a programmable metasurface. *Opt. Express* **2021**, *29*, 17258–17268. [[CrossRef](#)]
20. Shabanpour, J. Programmable anisotropic digital metasurface for independent manipulation of dual-polarized THz waves based on a voltage-controlled phase transition of VO₂ microwires. *J. Mater. Chem. C* **2020**, *8*, 7189–7199. [[CrossRef](#)]
21. Song, Z.Y.; Wei, M.L.; Wang, Z.S.; Cai, G.X.; Li, Y.N.; Zhou, Y.G. Terahertz Absorber with Reconfigurable Bandwidth Based on Isotropic Vanadium Dioxide Metasurfaces. *IEEE Photonics J.* **2019**, *11*, 4600607. [[CrossRef](#)]

22. Nouman, M.T.; Hwang, J.H.; Faiyaz, M.; Lee, K.J.; Noh, D.Y.; Jang, J.H. Vanadium dioxide based frequency tunable metasurface filters for realizing reconfigurable terahertz optical phase and polarization control. *Opt. Express* **2018**, *26*, 12922–12929. [[CrossRef](#)] [[PubMed](#)]
23. Qureshi, U.U.R.; Khan, M.I.; Hu, B. A Theoretical Proposal for an Actively Controlled Ultra-Wideband Absorber Based on Vanadium Dioxide Hybrid Metamaterials. *Appl. Sci.* **2022**, *12*, 10164. [[CrossRef](#)]
24. Xu, K.D.; Li, J.; Zhang, A.; Chen, Q. Tunable multi-band terahertz absorber using a single-layer square graphene ring structure with T-shaped graphene strips. *Opt. Express* **2020**, *28*, 11482–11492. [[CrossRef](#)]
25. Yang, J.; Chu, X.; Gao, H.; Wang, P.; Deng, G.; Yin, Z.; Lu, H. Fully Electronically Phase Modulation of Millimeter-Wave via Comb Electrodes and Liquid Crystal. *IEEE Antennas Wirel. Propag. Lett.* **2021**, *20*, 342–345. [[CrossRef](#)]
26. Yang, J.; Wang, P.; Shi, T.; Gao, S.; Lu, H.B.; Yin, Z.P.; Lai, W.E.; Deng, G.S. Electrically tunable liquid crystal terahertz device based on double-layer plasmonic metamaterial. *Opt. Express* **2019**, *27*, 27039–27045. [[CrossRef](#)]
27. Vasić, B.; Isić, G.; Beccherelli, R.; Zografopoulos, D.C. Tunable Beam Steering at Terahertz Frequencies Using Reconfigurable Metasurfaces Coupled With Liquid Crystals. *IEEE J. Sel. Top. Quantum Electron.* **2020**, *26*, 7701609. [[CrossRef](#)]
28. Wu, J.; Shen, Z.; Ge, S.; Chen, B.; Shen, Z.; Wang, T.; Zhang, C.; Hu, W.; Fan, K.; Padilla, W.; et al. Liquid crystal programmable metasurface for terahertz beam steering. *Appl. Phys. Lett.* **2020**, *116*, 131104. [[CrossRef](#)]
29. Liu, C.X.; Yang, F.; Fu, X.J.; Wu, J.W.; Zhang, L.; Yang, J.; Cui, T.J. Programmable Manipulations of Terahertz Beams by Transmissive Digital Coding Metasurfaces Based on Liquid Crystals. *Adv. Opt. Mater.* **2021**, *9*, 2100932. [[CrossRef](#)]
30. Fu, X.; Shi, L.; Yang, J.; Fu, Y.; Liu, C.; Wu, J.W.; Yang, F.; Bao, L.; Cui, T.J. Flexible Terahertz Beam Manipulations Based on Liquid-Crystal-Integrated Programmable Metasurfaces. *ACS Appl. Mater.* **2022**, *14*, 22287–22294. [[CrossRef](#)]
31. Tsai, Y.J.; Larouche, S.; Tyler, T.; Lipworth, G.; Jokerst, N.M.; Smith, D.R. Design and fabrication of a metamaterial gradient index diffraction grating at infrared wavelengths. *Opt. Express* **2011**, *19*, 24411–24423. [[CrossRef](#)]
32. Kang, J.H.; Choe, J.H.; Kim, D.S.; Park, Q.H. Substrate effect on aperture resonances in a thin metal film. *Opt. Express* **2009**, *17*, 15652–15658. [[CrossRef](#)] [[PubMed](#)]
33. Choe, J.H.; Kang, J.H.; Kim, D.S.; Park, Q.H. Slot antenna as a bound charge oscillator. *Opt. Express* **2012**, *20*, 6521–6526. [[CrossRef](#)] [[PubMed](#)]